

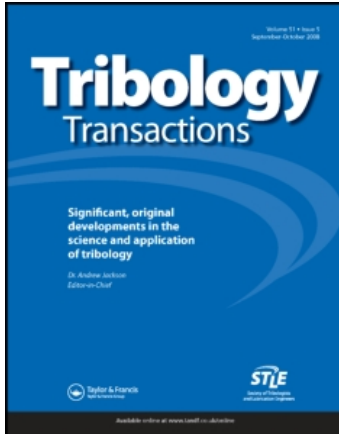
This article was downloaded by: [Arakere, Nagaraj K.][University of Florida]

On: 10 August 2010

Access details: Access Details: [subscription number 917341032]

Publisher Taylor & Francis

Informa Ltd Registered in England and Wales Registered Number: 1072954 Registered office: Mortimer House, 37-41 Mortimer Street, London W1T 3JH, UK



## Tribology Transactions

Publication details, including instructions for authors and subscription information:

<http://www.informaworld.com/smpp/title~content=t713669620>

### Critical Flaw Size in Silicon Nitride Ball Bearings

George A. Levesque<sup>a</sup>; Nagaraj K. Arakere<sup>a</sup>

<sup>a</sup> Mechanical & Aerospace Engineering, University of Florida, Gainesville, FL

First published on: 24 June 2010

**To cite this Article** Levesque, George A. and Arakere, Nagaraj K.(2010) 'Critical Flaw Size in Silicon Nitride Ball Bearings', Tribology Transactions, 53: 4, 511 – 519, First published on: 24 June 2010 (iFirst)

**To link to this Article:** DOI: 10.1080/10402000903491291

**URL:** <http://dx.doi.org/10.1080/10402000903491291>

## PLEASE SCROLL DOWN FOR ARTICLE

Full terms and conditions of use: <http://www.informaworld.com/terms-and-conditions-of-access.pdf>

This article may be used for research, teaching and private study purposes. Any substantial or systematic reproduction, re-distribution, re-selling, loan or sub-licensing, systematic supply or distribution in any form to anyone is expressly forbidden.

The publisher does not give any warranty express or implied or make any representation that the contents will be complete or accurate or up to date. The accuracy of any instructions, formulae and drug doses should be independently verified with primary sources. The publisher shall not be liable for any loss, actions, claims, proceedings, demand or costs or damages whatsoever or howsoever caused arising directly or indirectly in connection with or arising out of the use of this material.

# Critical Flaw Size in Silicon Nitride Ball Bearings

GEORGE A. LEVESQUE and NAGARAJ K. ARAKERE

Mechanical & Aerospace Engineering, University of Florida, Gainesville, FL 32611

*Silicon nitride balls, used in hybrid ball bearings, are susceptible to failure from fatigue spalls emanating from preexisting partial cone cracks that can grow under rolling contact fatigue (RCF). We simulate the range of three-dimensional nonplanar surface flaw geometries subject to RCF to calculate mixed mode stress intensity factors to determine the critical flaw size (CFS) or the largest allowable flaw that does not grow under service conditions. The cost of nondestructive evaluation (NDE) methods for silicon nitride balls scales exponentially with decreasing CFS and increasing ball diameter and can become a significant fraction of the overall manufacturing cost. Stress intensity factor variability is analyzed for variations of the location and orientation of the load relative to the crack, the geometry of load, and full-slip traction. The modeling techniques utilized in the creation of a three-dimensional (3D) finite element analysis (FEA) model is discussed and the maximum tensile contact periphery stress is examined for effect on crack driving force under RCF. The CFS results are presented as a function of Hertzian contact stress, traction magnitude, and crack size.*

## KEY WORDS

Partial Cone Crack; Fracture; Silicon Nitride; Friction; Stress Intensity Factor; Rolling Contact Fatigue; Hybrid Ball Bearings; Finite Element Modeling

## INTRODUCTION

The evaluation of a critical flaw size (CFS) is of immediate engineering relevance to the hybrid ball bearing industry toward defining refinement necessary for nondestructive evaluation methods for silicon nitride ball quality control. Also, a CFS can be applied for developing a fracture mechanics-based life prediction methodology for hybrid bearings. The performance of hybrid silicon nitride ( $\text{Si}_3\text{N}_4$ ) ball/steel raceway bearings has been shown to be superior to their all-steel predecessors (Miner, et al. (1); Tanimoto, et al. (2)). However, silicon nitride balls are sensitive to surface defects and can fail from fatigue spalls emanating from preexisting c-cracks or partial cone cracks (see Fig. 1), due to crack growth driven by rolling contact fatigue (RCF; Hadfield, et al. (3); Levesque and Arakere (4)). Silicon nitride exhibits fa-

vorable material properties for application in hybrid high-speed ball bearings such as high compressive strength, high hardness, a third of the density of steel, low coefficient of thermal expansion, and high corrosion and temperature resistance (Jahanmir (5)). Unfortunately, they also have low fracture toughness (4–6  $\text{MPa}\sqrt{\text{m}}$ ; Piotrowski and O'Brien (6)).

Silicon nitride ball manufacturing involves a lapping process to achieve the submicron ball finishing dimension and surface characteristics that produces (unavoidable) low-velocity ball collisions resulting in surface cracks nucleated by the radial tensile stress field, which is maximal at the contact periphery (Levesque and Arakere (4); Wang and Hadfield (7)). Partial cone or c-cracks are the result of the oblique impact of brittle spheres (Frank and Lawn (8)) and these cracks are considered the most damaging surface defect that limits ball life in hybrid bearings under service conditions (Evans (9); Hadfield, et al. (10)). C-cracks are more commonly observed in sphere-to-sphere collisions and they not only have nonplanar crack faces but also possess nonplanar crack tips, as opposed to the axisymmetric cone cracks that result from the normal collisions of spheres. Figure 1 illustrates the 3D nonplanar crack features of a c-crack. This increased complexity makes their shape more difficult to describe and, therefore, more complicated to analyze in any linear elastic fracture mechanics (LEFM) based analysis.

Though the flaws (illustrated in Fig. 1) can be readily induced and are generally present, methods for their detection prior to service are still in development. Development of a nondestructive evaluation (NDE) method is complicated because these cracks are often no more than 500  $\mu\text{m}$  (approximately the width of two human hairs) long on the surface and are difficult to find under a microscope. In addition, the material is nonconductive and only slightly translucent, which complicates inspection procedures. From a fracture mechanics and structural integrity perspective, the largest allowable surface flaw that does not propagate under RCF loading is of design significance and is termed the *critical flaw size*. The goal of this research is to present a systematic procedure to compute the CFS-based on fracture mechanics principles, RCF loading, and ball material properties. This analysis is driven by the cost of an NDE method for silicon nitride balls, which scales up very steeply with decreasing CFS and increasing ball diameter. Thus, the cost associated with NDE can become a significant fraction of the overall manufacturing cost of the silicon nitride ball.

Prior work has presented a qualitative and quantitative description of the range of possible partial cone crack shapes in three dimensions depending on the initial conditions of the

NOMENCLATURE

*a* = Axis dimension of ellipse in *x*-direction  
*a'* = Semi-elliptical crack semi-width  
*a\** = Axis dimension of revolved ellipse in the *x*-direction for c-crack creation  
*a<sub>c</sub>* = Radius of contact patch size  
*b* = Axis dimension of ellipse in *z*-direction  
*b'* = Semi-elliptical crack depth  
*b\** = Axis dimension of revolved ellipse in the *z*-direction for c-crack creation  
*ds* = Length element along the contour  $\Gamma$   
*E* = Young's modulus  
*E\** = Effective Young's modulus,  $E^* = (\frac{1-\nu_1^2}{E_1} + \frac{1-\nu_2^2}{E_2})^{-1}$   
*e* =  $e = \sqrt{1 - \alpha^2}$   
*G* = Strain energy release rate,  $G = \frac{1}{E}(K_I^2 + K_{II}^2) + \frac{2(1-\nu)}{E}K_{III}^2$   
*h* = *x*-Coordinate of crack at surface on *x* - *z* plane.  
*J* = Rice's contour integral  
*K<sub>eq</sub>* =  $K_{eq} = \{E[\frac{1}{E}(K_I^2 + K_{II}^2) + \frac{2(1-\nu)}{E}K_{III}^2]\}^{0.5}$   
*K<sub>eq</sub>\** =  $K_{eq}^* = K_{eq}/P_O\sqrt{a_c}$   
*K<sub>I</sub>* = Opening stress intensity factor  
*K<sub>I</sub>\** =  $K_I^* = K_I/P_O\sqrt{a_c}$   
*K<sub>II</sub>* = Sliding stress intensity factor  
*K<sub>III</sub>* = Tearing stress intensity factor  
*K<sub>th</sub>* = Threshold value which allows crack growth  
*k* = *z*-Coordinate of crack at surface on *x* - *z* plane

*m* = Ball mass  
*O* = Coordinate origin  
*P* = Total load  
*P<sub>o</sub>* = Max value of pressure in elliptical pressure dome  
*R* = Effective ball radius for a ball on ball interaction,  $R \equiv (\frac{1}{R_1} + \frac{1}{R_2})^{-1}$   
*r* = Distance from crack tip where *u*, *v*, and *w* are measured  
*T<sub>i</sub>* = Components of traction vector  
*u, v, w* = Crack face opening, sliding, and shearing displacements  
*u<sub>i</sub>* = Displacement vector components  
*V<sub>z</sub>* = Ball velocity to induce cracking  
*w* = Strain energy density  
*x<sub>d</sub>* = *x* Displacement of pressure distribution from coordinate origin  
*y<sub>d</sub>* = *y* Displacement of pressure distribution from coordinate origin  
 $\alpha$  = Aspect ratio of load (*b/a*)  
 $\Gamma$  = Arbitrary counterclockwise path around the crack tip  
 $\theta_{max}$  = Half the total amount which the crack subtends a circle  
 $\mu$  = Friction coefficient  
 $\nu$  = Poisson's ratio  
 $\rho$  = Material density  
 $\sigma_c$  = Critical max periphery stress to induce cracking  
 $\phi_{pl}$  = Angle of principle plane

interaction (coefficient of friction and contact patch size) during oblique spherical contact (Levesque and Arakere (4)). With this range of possible nonplanar shapes characterized, they may be analyzed under RCF conditions that are seen in service, to determine which physical effects have the largest impact on crack tip displacement. Rolling elements are manufactured with silicon nitride because of the severe RCF conditions the material can

withstand. These conditions are severe for any preexisting surface flaws that exist. For example, in the case of a mainshaft jet engine bearing inner ring rotating at 15,000 rpm, and as a worst-case scenario considering that the c-crack lies along the ball track (see Fig. 2), the crack can experience in excess of 90,000 fatigue cycles per minute (1,500 Hz) or 5.4 million cycles/hour. Furthermore, as the c-crack passes through the contact patch, the crack tip experiences a mixed-mode  $\Delta K$  loading at every point along the crack front. We present the effects of the location and orientation of

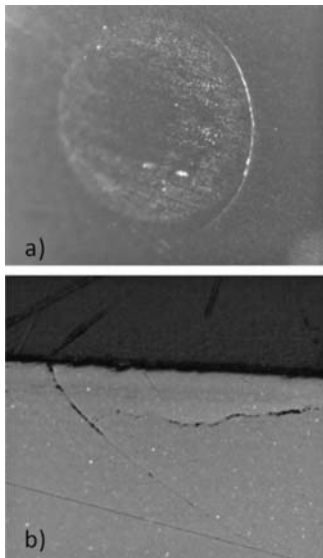


Fig. 1—Images of artificially induced c-cracks: (a) ball surface view and (b) a subsurface cross section extending into the material (courtesy of the Timken Company).

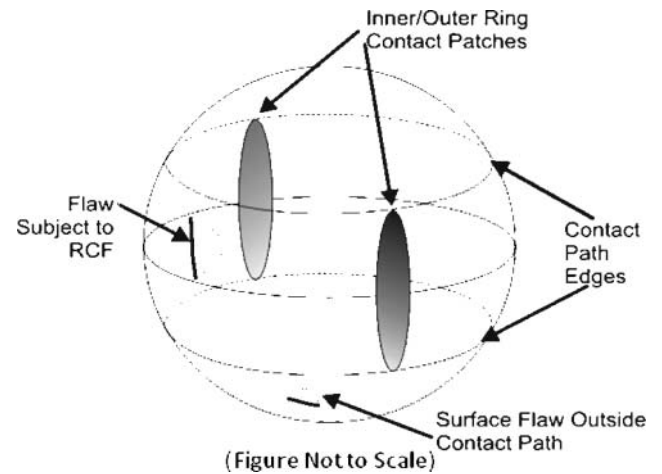


Fig. 2—The elliptic contact patches on the ball surface and the band that they remain in. Cracks inside and very close to this region (assuming a fixed contact angle and attitude of ball rotation) will experience RCF.

the load relative to the crack, the geometry of load, the geometry of the crack, and the respective effects on crack tip stress intensity factors (SIFs) and, therefore,  $\Delta K$ . There is no published work concerning an elliptical Hertzian contact load inducing RCF for nonplanar c-cracks, which is what is most often seen in service applications. Herein, we analyze the discussed effects on the SIFs in the ball bearing system and the process of extracting them.

**ANALYTICAL PROCEDURE**

**Crack Geometries Induced by the Oblique Interaction of Silicon Nitride Balls**

The c-cracks produced during oblique interaction have multiple geometric features that need to be understood before modeling is undertaken. It can be shown that the crack size scales with the ball radius,  $R$ , and that the velocity needed to induce cone cracks is very low and can be shown to be proportional to  $R^3$  (see the Appendix). Also, it is noteworthy that the angular extensions of the c-cracks have been observed to be roughly 90 to 120° (Levesque and Arakere (4); Wang (11)). However, cracks that are the result of normal indentation of spheres have a weak correlation about the depth to which they extend into the material and exhibit considerable variation even for similar indentation conditions (Johnson (12)). Avoiding generalities, the range of the geometry of cracks produced by ball-on-ball collisions was established in a previous paper by the authors, using a stress-state and numerical iterative growth and compared with experimental images (Levesque and Arakere (4)). The angles to which the crack extends subsurface have already been bracketed within an established range in the same reference. The resultant shape from these oblique interactions is complex and other prior works characterized the approximately modeled crack geometry with sets of parametric equations (Wang (11)). However, the complexity of the shape leads to a difficulty in generalizing results and in finding which geometry of crack will be the most severely affected by RCF.

With this information in mind, we can model the c-crack geometry as a partial cone, or a partial frustum, whose dimensions are limited by inequalities that are equations of an offset cylinder. In other words, the shape is an axially revolved quarter ellipse with limitations to its extension in the  $r$ - and  $\theta$ -direction (considering cylindrical coordinates; see Fig. 3).

$$z = \frac{1}{a^*b^*} \sqrt{a^{*2} - (\sqrt{x^2 + y^2} - h)^2} + k \tag{1}$$

where

$$-\frac{1}{2}\theta_{range} \leq \tan^{-1}\left(\frac{y}{x}\right) \leq \frac{1}{2}\theta_{range} \tag{2}$$

$$h - a^* \leq \sqrt{x^2 + y^2} \leq \frac{1}{2} \sec\left(\tan^{-1}\left(\frac{y}{x}\right)\right) \times \left[ \frac{1}{h - a^*} - \sqrt{2} \sin\left(\frac{1}{2}\theta_{range}\right) + (h - a^*) \right] \tag{3}$$

where  $a^*$  and  $b^*$  are the axes of the ellipse on the  $x$ - and  $z$ -axes, respectively;  $h$  and  $k$  are the  $x$  and  $z$  coordinates of the center of the quarter ellipse, respectively; and  $\theta$  is used to denote the

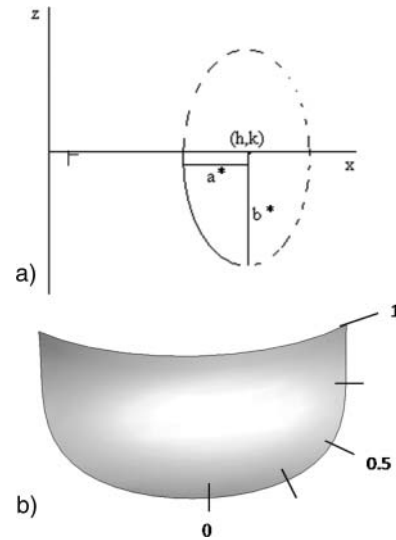


Fig. 3—(a) The coordinate system used in the equations to plot the c-crack and (b) the rendered 3D crack with notation for the SIF plots to be discussed.

fraction of a circle that the crack is seen to be on the surface of the specimen (see Fig. 3).

**Finite Element Analysis Modeling of a 3D Surface Flaw**

The shape of the crack is critical to understanding the difficulties of generating an adequate mesh for finite element analysis (FEA). In order to accurately model a crack for SIFs, we utilize quadratic elements to account for the large gradients of stress that occur throughout the model as a result of the Hertzian contact loading. To accurately model the crack tip stress, we use collapsed hexahedral elements at the tips with the mid-side nodes moved to the quarter-point (Andersson (13)). Because hexahedral elements are utilized at the tip,  $C_1$  continuity of the shape functions is maintained, which is desirable especially if SIFs are intended to be extracted in the region just surrounding the crack tip. It is noteworthy to mention that others have developed methods to extract SIFs from tetrahedral based meshes, which simplifies meshing and remeshing in the instance of crack growth, but there is still much variability in the method (Rajaram, et al. (14)). However, it would be difficult to create a mesh that would be made of all hexahedral elements and avoid distorted warning elements considering that the geometry is curvilinear and closed. Through benchmark analyses, types of meshes and their SIFs were tested against previously established solutions (like that of Newman and Raju (15)). As a result, we could create a tube of elements that were hexahedral, about the crack tip region but were tied to a bordering tetrahedral region that meshed the majority of the cracked body and maintain SIF accuracy.

SIF extraction from this mesh is feasible through a few methods (including stress matching and virtual crack extension), but the most appropriate approach for our analyses is via crack tip opening displacement (CTOD) correlation because it accounts for the effects of all physical phenomena without a need to change its formulation (as in contour integral, energy-based methods).

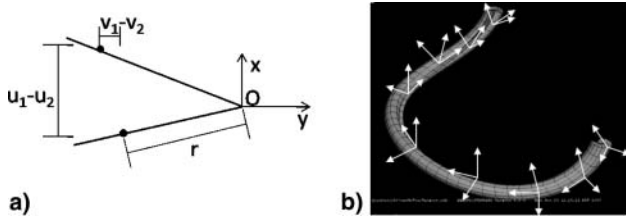


Fig. 4—Illustration of (a) displacement correlation variables around an opening two-dimensional crack and (b) the coordinate systems are different for each point near the crack tip at a few element borders. (Figure available in color online.)

The equations for displacement correlation can be written as:

$$K_I = \frac{E}{4(1-\nu^2)} \sqrt{\frac{2\pi}{r}} (u_1 - u_2) \quad [4a]$$

$$K_{II} = \frac{E}{4(1-\nu^2)} \sqrt{\frac{2\pi}{r}} (v_1 - v_2) \quad [4b]$$

$$K_{III} = \frac{E}{4(1-\nu^2)} \sqrt{\frac{2\pi}{r}} (w_1 - w_2) \quad [4c]$$

where  $E$  and  $\nu$  are the Young's modulus and Poisson's ratio;  $u$ ,  $v$ , and  $w$  are the three displacements in the directions normal to the crack face, in the direction of the continuing crack plane normal to the tip, and tangent to the crack tip, respectively; and  $r$  is the distance from the crack tip, where these displacements are measured. Figure 4(a) illustrates the CTOD coordinate system. Figure 4(b) shows the 3D displacement vectors at the tip of the nonplanar c-crack mesh.

The FEA model represents a computationally intense effort due to the dense mesh (for capturing the Hertz stress gradients) and implementation of quadratic elements (for moving the mid-side node of the tip elements to the quarter point, preserving the  $1/\sqrt{r}$  singularity at the crack tip) and accounting for contact accuracy. Mesh refinement for Hertz contact problems has been visited in other works (Gu, et al. (16)) usually for stress calculations. Here the displacements are of primary importance, especially those in the crack-tip vicinity. We have performed a mesh refinement study in the tensile region on the contact periphery and established guidelines for accurate determination of SIFs. The mesh density utilized is about 50 elements along the crack to the tip where the hexahedral region has four to seven rings of elements in the contour region, meaning that for our application each element near the tip is  $\sim 10 \mu\text{m}$  wide (which is the length of the longest grains in TSN-03 NH silicon nitride). Contact of the crack faces is defined by using a surface-based contact definition with no friction where a direct, iterative solver is used to achieve accurate displacement and stress field solutions.

The direct iterative solver must be used because the accuracy in displacement results required for adequate SIF calculations is high. The direct iterative solver is the most accurate solver available in ABAQUS (Dessault Systèmes (17)). The mesh refinement previously established is based upon (a) refinement that the Hertz contact requires for adequate resolution and (b) refinement in the vicinity of the crack tip necessary for accurate displacements needed for SIF computation.

Loading is done via FORTRAN user subroutines DLOAD and UTRACLOAD for the normal and traction loads. The equations to describe the pressure distributions can be written as:

$$p(x, y) = P_o \sqrt{\frac{(x - x_d)^2}{a^2} - \frac{(y - y_d)^2}{b^2}} \quad [5]$$

and

$$f(x, y) = \mu p(x, y) \quad [6]$$

where  $x_d$  and  $y_d$  are the distances from the global coordinate system to the load center,  $a$  and  $b$  are the dimensions of the ellipse along these dimensions, and  $\mu$  is the friction coefficient for the moving load in a full-slip interaction (see Fig. 5).

### MIXED-MODE SIFS DUE TO RCF

For generalization, the trends observed in the SIFs for each of the possible physical parameters should be investigated and quantified. For example, if the max Hertzian pressure is increased, the SIFs are mostly observed to directly scale with the value of  $P_o$ . In some mainshaft ball bearing applications, maximum Hertzian contact pressure,  $P_o$ , is in the range of 1.7–2.8 GPa (250–412 Kpsi) (380–412 kpsi). We present SIF results at the upper end of that range, at 2.8 GPa, to obtain conservative estimates on CFS for ball material. For the orientation in Fig. 6 without traction, the linear effect of max pressure on SIFs is demonstrated in Fig. 7. This information may be applied by others in the field who require SIF calculations for similar phenomena but different magnitudes of pressure in their contact ellipse.

In the two-dimensional case, the width of the contact, the angle of the crack, and the depth of the crack are enough parameters to define an RCF model (Bogdanski and Trajer (18)). However, for 3D analysis, the model must be characterized by the load aspect ratio and specific crack dimension, making generalization of results difficult.

Now we turn to an analysis of SIFs as a function of approaching load, illustrated in Fig. 8. There are multiple static steps to analyze these c-cracks under an RCF cycle (or single passage of the load rolling over the crack). As the load approaches the  $K_I$  SIF increases until the load is very close to the crack tip, resulting in crack closure. At this point,  $K_I$  rapidly decreases to zero as the contact patch moves directly over the crack. As the contact patch advances further the crack tip opens due to the influence of the maximum tensile stress on the trailing edge of the load. Though  $K_I$  reaches a second maximum in the trailing periphery edge, it is not as high as that of the approaching edge because the crack angle (illustrated in Fig. 6) is such that the depression from the load has a tendency to cause the crack to close as shown in Fig. 8. As the load moves away from the crack, all the SIFs eventually decay to zero. In Fig. 8, the relative orientation of crack tip and load allows for influence of the load at 3a but  $K_I$  and  $K_{III}$  decay quickly thereafter. For design application, we are using an effective stress intensity parameter that embodies all modes of crack deformation as:

$$K_{eq} = \sqrt{EG} = \left\{ E \left[ \frac{1}{E} (K_I^2 + K_{II}^2) + \frac{2(1-\nu)}{E} K_{III}^2 \right] \right\}^{0.5} \quad [7]$$

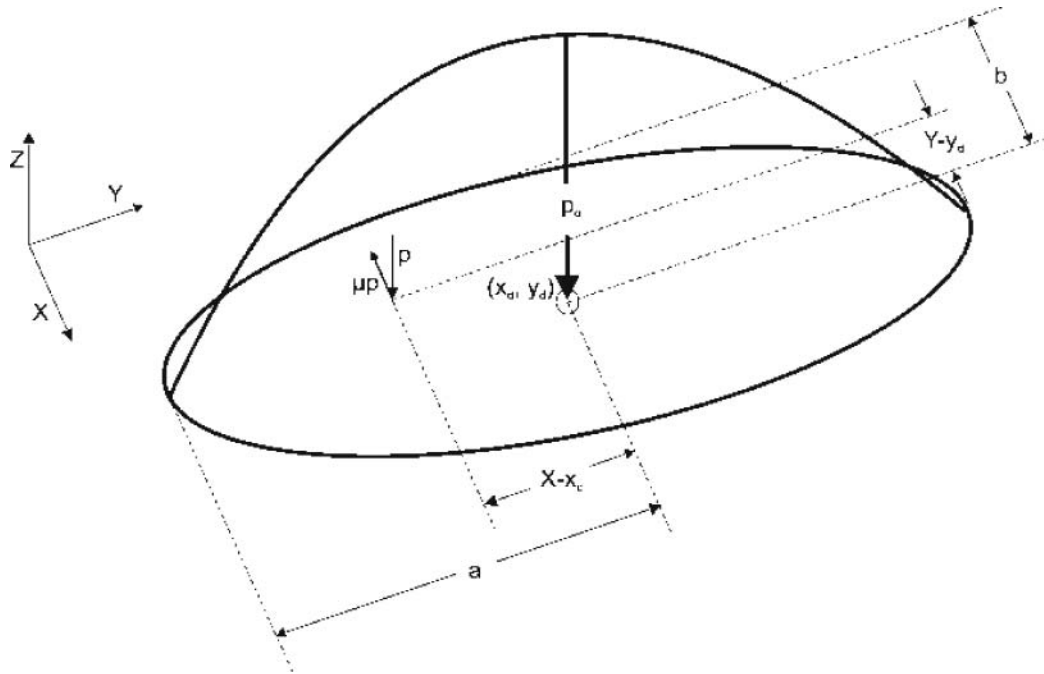


Fig. 5—Elliptical Hertzian contact load coordinate system and variables for elliptical load simulation.

This representation of the three modes of crack-tip displacement was chosen due to its physical basis in fracture mechanics (because it utilizes the strain energy release rate,  $G$ ; Anderson (19)).

The most severe orientation of a purely normal load (i.e., no traction load) is such that the periphery stress is near the crack on the side where the crack is oriented (see Fig. 6). However, the distance to the center of the approaching load ( $x_d$ ) where max SIFs are calculated is affected by the crack angle.

**EFFECT OF THE VARIATION OF LOAD ELLIPTICITY ON SIFs**

The ellipticity of the contact patch also influences the induced SIFs. For a generalized Hertzian elliptical contact seen in a ball bearing the ellipticity ratio ( $b/a$ ) can vary depending on the raceway curvatures, speed, radial, and thrust loads. A nearly circular contact patch is often seen in RCF test setups like the ball on rod test, the four- and five-ball tests, v-ring test, and more. Also, if  $b/a$  is very small, the contact can be reminiscent of a line contact.

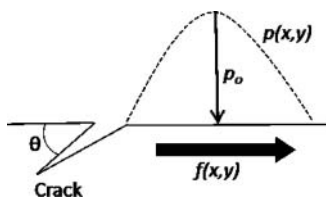


Fig. 6—The cross section of the general worst-case orientation with traction for crack-tip deformation. Here the traction direction acting on the silicon nitride surface is indicated and considerations of relative movement must be based on which surface is driving each contact, which is different for inner and outer raceway interactions.

Because the crack is moving with the rotating ball, the relative orientation of crack and load can vary greatly. The effect of ellipticity of load on the SIFs from the semi-minor axes is studied in Fig. 9. The circular case yields comparatively higher SIFs. This is due to the nature of the stresses that circular loads can produce at their periphery (Johnson (12)).

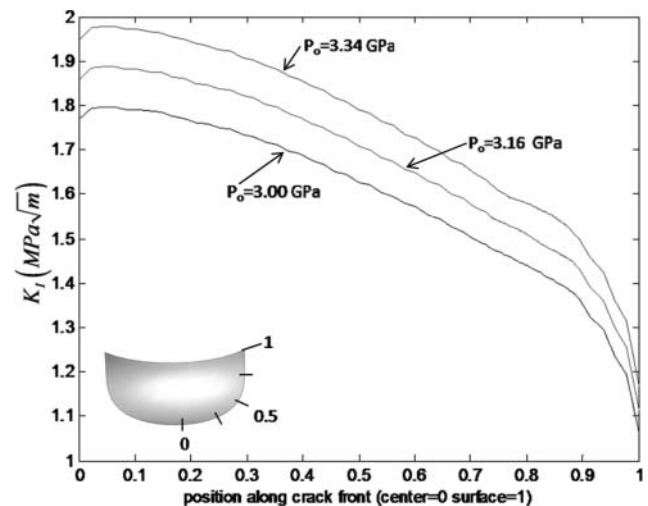


Fig. 7— $K_I$  stress intensity factor for a circular load ( $a_c = 250 \mu\text{m}$ ) near a c-crack (width =  $250 \mu\text{m}$ , vertical depth =  $75 \mu\text{m}$ , and an angle of  $28^\circ$  to the surface) with a variation in the max pressure magnitude. The effect of a scalar increase in pressure is a near scalar increase in  $K_I$ . (Figure available in color online.)

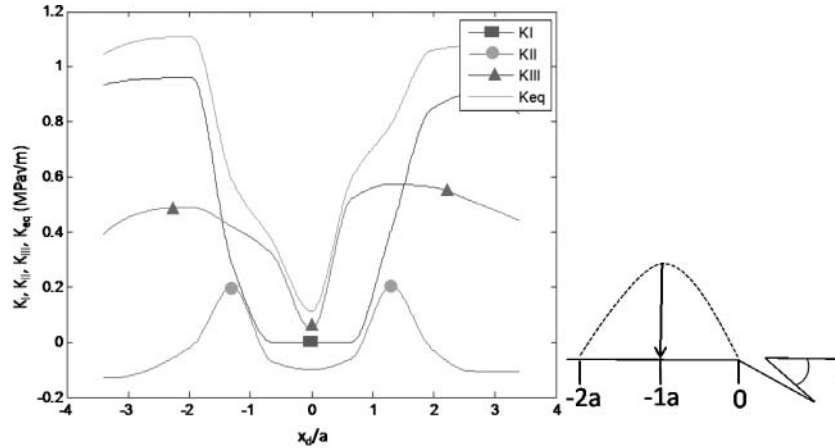


Fig. 8—A plot of the three SIFs as a function of moving load of  $P_o = 2.8$  GPa. When  $\text{abs}(x_d/a) = 1$ , the load is just on the edge of the crack and the coordinate system is oriented where the crack breaks the surface. The maximum SIFs along the crack front are plotted and they occur around  $x_d/a = -1.7$  for this geometry crack and load.(Figure available in color online.)

**COMPARISON OF C-CRACKS AND SEMI-ELLIPTICAL CRACKS**

The range of possible crack shapes and sizes has been established by Levesque and Arakere (4). The complex nonplanar 3D geometry of the c-crack requires parameters such as crack depth and angle, which are difficult to measure, and a function that represents the position of the surface and inequalities to indicate the end of the crack (see Eqs. [1]–[3]). Also, the NDE inspection procedures can only detect the chord length of the crack on the surface. Much of this issue could be resolved by comparing c-cracks to a semi-elliptical flaw that is fully classified by three parameters

(depth, width, and angle of inclination). The semi-elliptical crack also yields higher SIFs, for the same peak Hertz stress,  $P_o$ , leading to a conservative analysis and then the feasibility of simulation becomes much more accessible to other workers in the field. With this in mind, comparison of SIFs for the same orientation of elliptical contact load of both a c-crack and a semi-elliptical surface crack of similar width, depth, and angle toward the surface was completed. Results are displayed in Fig. 10.

When we compare the SIFs, we can notice considerable divergence in their values even though they occur in the same relative orientation to the load. However, the maxima and minima of each, though at different locations, are quite similar. As a result of the complex geometry and loading, all three modes of crack tip deformation are present. Modeling and experimental efforts need

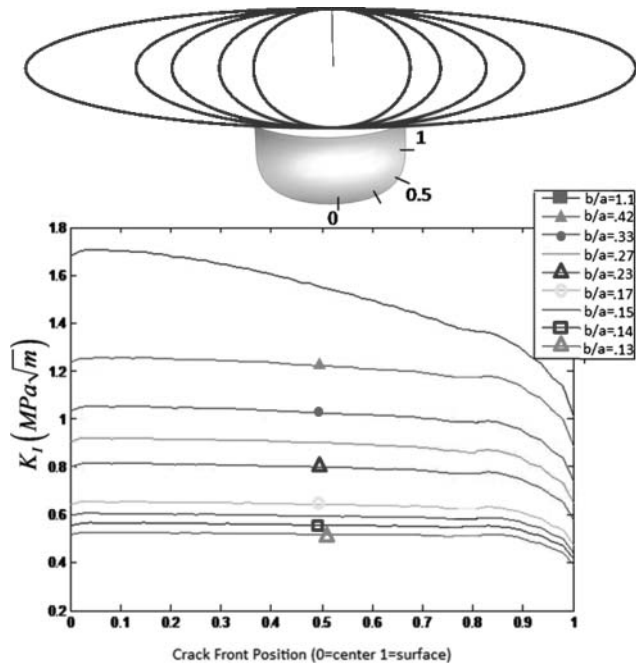


Fig. 9—The effect of the ellipticity of the load on the SIFs on the semi-minor axis of the ellipse for  $P_o = 2.8$  GPa (412 kpsi).(Figure available in color online.)

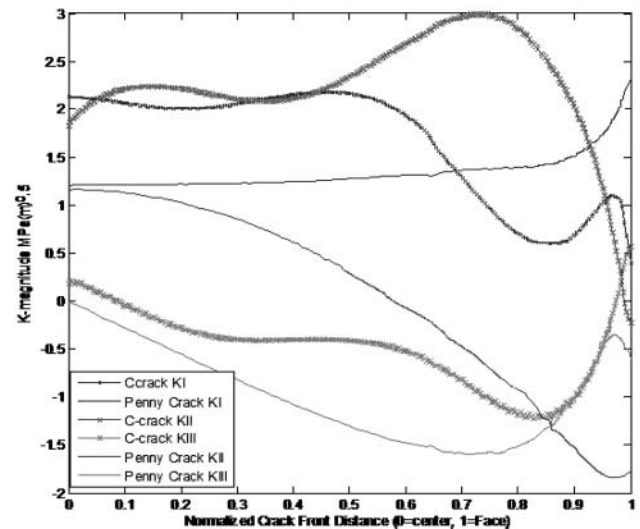
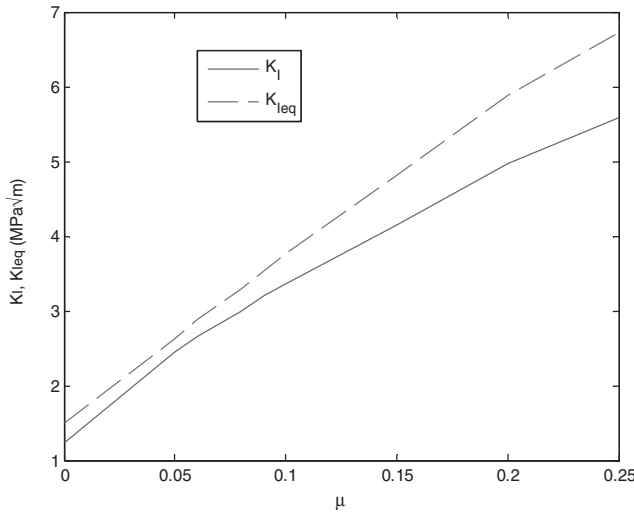


Fig. 10—Superimposed SIFs for a c-crack and penny crack of similar dimensions under elliptical load ( $a = 360 \mu\text{m}$ ,  $b = 120 \mu\text{m}$ , and  $P_o = 3.7$  GPa [540 kpsi]) where the surface crack is tangent to the semi-minor edge of the contact patch.(Figure available in color online.)



**Fig. 11**—The max  $K_I$  found on the crack front of a semi-elliptical flaw that is  $30^\circ$  to the surface and has  $a' = 250$   $b' = 75$  as a function of varying friction coefficients on an elliptical contact patch in full slip for  $P_o = 3.7$  GPa. (Figure available in color online.)

to collaborate to determine the best mixed-mode parameter for crack growth of brittle materials under these types of conditions for future design purposes.

### THE EFFECT OF TRACTION

Under elastohydrodynamic (EHD) lubrication conditions in a ball bearing, the effective friction coefficient at the contact is typically in the 0.05–0.09 range. Although the coefficient of friction appears to be low, we will show that it has a significant effect on the maximum SIFs reached. The direction of traction also becomes important. When traction is incorporated, we see that the worst-case load moves immediately next to the crack and that the SIFs increase substantially (see Fig. 6). If the traction direction is reversed, the worst-case load jumps to the opposite side of the crack where the tensile stress field has the most effect. (It should be noted that this position will not have as high SIFs as that on the opposing side because the normal load only contributes to crack closure on that side of the crack.)

During RCF, the elliptical contact patch induces both normal and traction forces onto the ball surface. Because the bearings of interest are lubricated, the interfacial contact is in full slip (a hydrodynamically lubricated contact) and the amount of traction on the surface is limited by the shearing properties of the lubricant that is in application. For the most part, we find that  $\mu = 0.05$ – $0.09$  is an acceptable range for high-speed bearing applications. The traction force is parametrically varied and the max stress intensity factor values along the front are plotted in Fig. 11.

It is quite apparent that the slope of the increasing SIFs is quite steep as the traction force is increased. For silicon nitride, the fracture toughness ( $K_{Ic} = 6.0$  MPa√m) is reached when  $\mu = 0.2$  and indicates that the friction coefficient is a critical variable to evaluate a CFS for ball bearing inspection. The reason for the strong influence of the friction coefficient is that the tangential traction force in the right direction has a pronounced effect on the crack opening force. In addition, there are high nor-

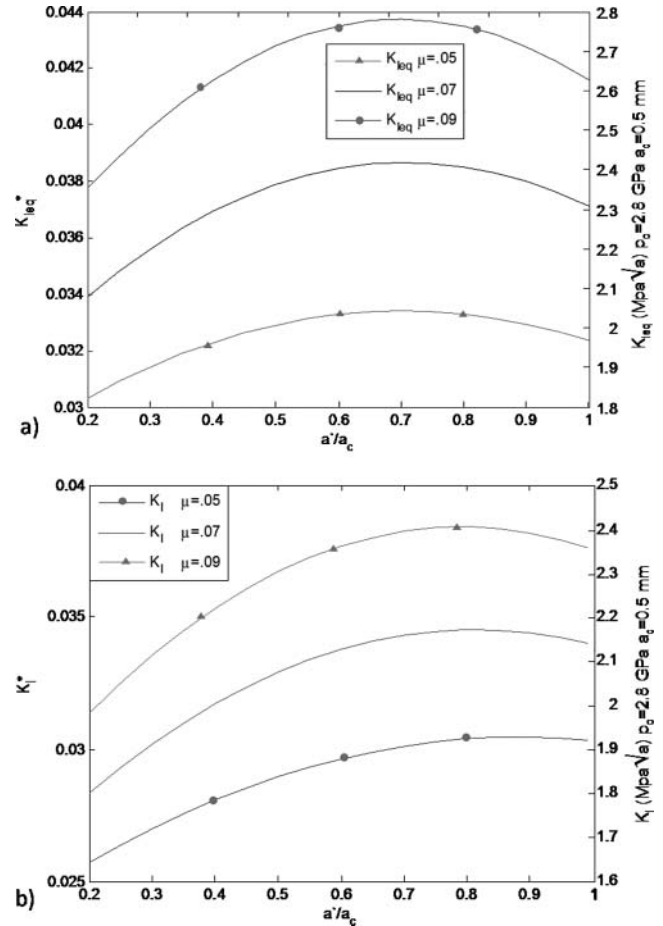


**Fig. 12**—The nondimensionalized crack semi-width plotted against (a) the max  $K_{I,eq}$  and (b) the max  $K_I$  where nondimensional units are on the left and in MPa√m for  $p_o = 2.8$  GPa and  $a_c = 0.5$  mm on the right. The SIFs are nondimensionalized by dividing the calculated values by  $P_o/a_c$ . (Figure available in color online.)

mal loads that are directly contributing to a traction load according to  $f = \mu P(x, y)$  (where, for example, for a normal contact stress of 2,600 MPa [ $\sim 380$  ksi], for  $\mu = 0.07$ , the tangential traction stress of 180 MPa [ $\sim 27$  ksi] is contributing to crack opening).

### CRITICAL FLAW SIZE EVALUATION RESULTS

If the operating conditions of a bearing are known, and the material properties (especially the  $K_{th}$  for initiating crack growth) are established, then a CFS (or flaw size so small that it experiences crack tip loading below the  $K_{th}$  threshold value under the operating conditions) can be found. Our models can be generalized for exactly this application. For example, we have established that the SIFs scale linearly with the max pressure,  $P_o$ , of the elliptical contact patch. We have also established that a circular load will produce higher SIFs than the commonly found elliptical dimensions. In addition, we have noticed that similar magnitudes of maximum SIFs across the crack front of c-crack and semi-elliptical flaws occur under identical loading conditions. We have also established that traction has a significant effect on the SIFs for the RCF of surface flaws. With all these facts in mind, we can run models that simulate a decreasing crack size near a circular

load and plot the change in the SIFs as a function of the changing crack size. By nondimensionalizing the SIFs with respect to the max contact pressure ( $K_I^* = K_I/P_o\sqrt{a_c}$ ), we can generalize the results. The crack dimensions chosen were based on what is commonly observed in experiments. In this case, we have modeled cracks that have an aspect ratio of 0.3 and are angled 30° from the surface. Figure 12 displays the results. To utilize this graph, all that is needed is the effective threshold value  $K_{th}$  of the material, under mixed-mode loading, and the CFS can then be looked up for design purposes after dimensionalizing the data for specific applications. For example, for  $P_o = 2.8$  GPa,  $\mu = 0.07$ , and  $a_c = 0.5$  mm, if  $K_{th} = 2.3$  MPa $\sqrt{m}$ , then the CFS is 500  $\mu$ m. The material property  $K_{th}$  can also be determined via RCF testing of c-cracked balls for specific contact loading conditions. For example, if a ball with a crack of  $a' = 350$   $\mu$ m and loading conditions of  $P_o = 2.8$  GPa,  $\mu = 0.07$ ,  $a_c = 500$   $\mu$ m, then  $K_{th} = 2.4$  MPa $\sqrt{m}$ .

## CONCLUSIONS

The evaluation of a CFS has important engineering relevance toward defining limits for NDE methods for silicon nitride ball quality control, for reducing the cost of ball inspection, and for developing a fracture mechanics-based life prediction methodology for hybrid bearings. To this end, we have analyzed complex surface cracks present in silicon nitride balls used in hybrid bearings subject to RCF, using 3D FEA and fracture mechanics principles. Though the relative position of load affects the SIFs at any given instant, the max SIFs, used in a  $\Delta K$  calculation, are observed in trends and were utilized in the determination of the smallest allowable CFS. These observations include:

- Surface cracking can be induced in silicon nitride ball collisions with low velocities of  $\sim 16$  cm/s.
- Surface crack dimensions that result from collisions can be shown to scale linearly with ball radius,  $R$ , and the velocity to induce cracking with the cube of the ball radius,  $R^3$ .
- C-cracks are a complex shape that can be modeled through iterative growth, or solid modeling, where the shape has been characterized by equations.
- Maximum Hertzian stress,  $P_o$ , scales the SIFs for c-cracks in balls subject to RCF in a nearly linear fashion.
- Surface traction between the ball and the raceway and its direction has a significant detrimental effect on SIFs and crack driving force.
- The max SIFs are seen while the crack is on the edge of a circular load when compared to approaching elliptical loads.
- The semi-elliptical crack is simpler to model and does exhibit similar magnitudes of SIFs, which are necessary for  $K_{th}$  calculations to determine a CFS.
- CFS can be determined from plot of SIFs versus crack dimension (Fig. 12) by looking up the appropriate mixed-mode effective threshold SIF value,  $K_{th}$ , which can be determined via RCF testing of c-cracked silicon nitride balls for specific contact loading conditions.

## ACKNOWLEDGEMENTS

Robert Wolfe, Manager, Materials Technology, Timken Company, Canton, Ohio, is thanked for many helpful discussions on

RCF loading of silicon nitride balls and the crack images. This work has been supported by the Air Force Research Labs under contract #F33615-03-D-2353-0003 and by the Timken Company, Canton, Ohio.

## REFERENCES

- (1) Miner, J. R., Dell, J., Galbato, A., and Ragen, M. A. (1996), "F-117-PW-100 Hybrid Bearing Ceramic Technology Insertion," *ASME Journal of Engineering for Gas Turbines and Power*, **118**, pp 434-442.
- (2) Tanimoto, K., Kajihara, K., and Yanai, K. (2000), "Hybrid Ceramic Ball Bearings for Turbochargers," *SAE Paper No. 2000-01-1339*.
- (3) Hadfield, M., Stolarski, T., Cundill, R. T., and Horton, S. (1993), "Failure Modes of Ceramic Elements with Ring Crack Defects," *Tribology International*, **26**, pp 157-164.
- (4) Levesque, G., and Arakere, N. (2008), "An Investigation of Partial Cone Cracks in Silicon Nitride Balls," *International Journal of Solids and Structures*, **45**(25-26), pp 6301-6315.
- (5) Jahanmir, S. (1994), *Friction and Wear of Ceramics*, Marcel Dekker: New York.
- (6) Piotrowski, A. E., and O'Brien, M. J. (2006), "A Novel Test Method to Measure the Fracture Toughness of Ceramic Balls Used in Bearings," *Fatigue and Fracture in Engineering of Materials and Structures*, **29**, pp 558-572.
- (7) Wang, Y., and Hadfield, M. (2000), "The Influence of Ring Crack Location on the Rolling Contact Fatigue Failure of Lubricated Silicon Nitride: Experimental Studies," *Wear*, **243**, pp 157-166.
- (8) Frank, F. C., and Lawn, B. R. (1967), "On the Theory of Hertzian Fracture," *Proceedings of the Royal Society of London Series A*, **299**, pp 291-306.
- (9) Evans, A. G. (1983), In: Riley, P. L. (Ed), *Progress in Nitrogen Ceramics*, Martinus Nijhoff Publishers: The Netherlands, p 595.
- (10) Hadfield, M., Stolarski, T. A., Cundill, R. T., and Horton, (1993), "Failure Modes of Ceramics in Rolling Contact," *Proc. Roy. Soc. Lond. Ser. A*, **443**, pp 607-621.
- (11) Wang, Y. (2000), *Failure Modes of Silicon Nitride Rolling Elements with Ring Cracks*, Ph.D. Thesis, Bournemouth University, UK.
- (12) Johnson, K. L. (1987), *Contact Mechanics*, Cambridge Press: Cambridge.
- (13) Andersson, M. (1996), "Stress Distribution and Crack Initiation for an Elastic Contact Including Friction," *International Journal of Solids and Structures*, **33**, pp 3673-3696.
- (14) Rajaram, H., Socrate, S., and Parks, D. M. (2000), "Application of Domain Integral Methods Using Tetrahedral Elements to the Determination of Stress Intensity Factors," *Engineering Fracture Mechanics*, **66**(5), pp 455-482.
- (15) Newman, J. C., and Raju, I. S. (1981), "An Empirical Stress-Intensity Factor Equation for the Surface Crack," *Engineering Fracture Mechanics*, **15**, p 185.
- (16) Gu, P., Nordlund, P., Asaro, R. J., and Uang, C. M. (2005), "Crack Face Contact, Frictional Sliding and Mesh Design Flexibility," *Communications in Numerical Methods in Engineering*, **21**, pp 209-217.
- (17) Dessault Systèmes. (2007), *ABAQUS Theory Manual*, Dessault Systèmes: Providence, RI.
- (18) Bogdanski, S., and Trajer, M. (2005), "A Dimensionless Multi-Size Finite Element Model of a Rolling Contact Fatigue Crack," *Wear*, **258**, pp 1265-1272.
- (19) Anderson, T. L. (2005), *Fracture Mechanics: Fundamentals and Applications*, Taylor & Francis Group: Boca Raton, FL.

## APPENDIX: THE NORMAL INDENTATION OF BRITTLE SPHERES

Before determining the critical flaw size, the size of the cracks can be discussed practically. As discussed above, the fracture toughness of Si<sub>3</sub>N<sub>4</sub> is low (about 6 MPa $\sqrt{m}$ ; Piotrowski and O'Brien (6)), and the resultant velocity to induce cone cracking of normally colliding balls is low. The velocity to induce cracking,  $V_z$ , has been derived by Levesque and Arakere (4) for normal ball collisions as:

$$V_z = \frac{51\sqrt{5}}{50} \frac{\pi\sigma_c^{\frac{5}{2}} R^{\frac{3}{2}} m^{\frac{1}{2}}}{E^{*2}} \quad [A1]$$

and determines that 16 cm/s is a sufficient velocity to crack normally interacting 6.38 mm (0.5 in.) diameter balls. Substituting for the ball mass,  $m = \rho V = \rho(\frac{4}{3}\pi R^3)$ , in Eq. [A1] yields:

$$V_z = \frac{51}{25} \sqrt{\frac{5}{3}} \frac{\pi^{\frac{1}{2}} \rho^{\frac{1}{2}} \sigma_c^{\frac{5}{3}} R^3}{E^{*2}} \quad [\text{A2}]$$

Equation [A2] shows that the velocity to induce cracking is proportional to  $R^3$ . The effect that the radius of the ball has on the size of the crack can also be calculated because contact patch radius is given by:

$$a_c = \left( \frac{3PR}{4E^*} \right)^{\frac{1}{3}} \rightarrow P = \frac{4E^* a_c^3}{3R} \quad [\text{A3}]$$

The max Hertzian contact pressure for a ball on ball interaction is

$$p_o = \left( \frac{3P}{2\pi a_c^2} \right) \rightarrow \text{substituting } P_o = \frac{2E^* a_c}{\pi R} \quad [\text{A4}]$$

From prior work (Levesque and Arakere (4)), cracking will occur when a maximum stress value is reached and for Hertzian contacts the max stress value in the half-space is located just outside the contact region. For cone cracking to start at the periphery, the value of the maximum principal stress that must be exceeded is determined by

$$\sigma_{\max} = \frac{1-2\nu}{3} p_o \rightarrow p_o = 6.8\sigma_{\max} \quad [\text{A5}]$$

Substituting Eq. [A4] and rearranging results in

$$a_c = \frac{3.4\pi R \sigma_{\max}}{E^*} \quad [\text{A6}]$$

Therefore, the contact patch size, and therefore the crack radius, scales linearly with ball radius ( $R$ ), assuming that the two interacting balls have the same radius.